# Excited State Dynamics of the Isolated Green Fluorescent Protein Chromophore Anion Following UV Excitation

**ARTICLE** *in* THE JOURNAL OF PHYSICAL CHEMISTRY B · FEBRUARY 2015

Impact Factor: 3.3 · DOI: 10.1021/acs.jpcb.5b01432 · Source: PubMed

THE JOURNAL OF PHYSICAL CHEMISTRY B

Article

pubs.acs.org/JPCB

# Excited State Dynamics of the Isolated Green Fluorescent Protein Chromophore Anion Following UV Excitation

Christopher W. West, James N. Bull, Alex S. Hudson, Steven L. Cobb, and Jan R. R. Verlet*

Department of Chemistry, Durham University, Durham, DH1 3LE, United Kingdom

Supporting Information

**ABSTRACT:** A combined frequency-, angle-, and time-resolved photoelectron spectroscopy study is used to unravel the excited state dynamics following UV excitation of the isolated anionic chromophore of the green fluorescent protein (GFP). The optically bright $S_3$ state, which is populated for $h\nu > 3.7$ eV, is shown to decay predominantly by internal conversion to the $S_2$ state that in turn autodetaches to the neutral ground state. For $h\nu > 4.1$ eV, a new and favorable autodetachment channel from the $S_2$ state becomes available, which leads to the formation of the neutral in an excited state. The results indicate that the UV excited state dynamics of the GFP chromophore involve a number of strongly coupled excited states.

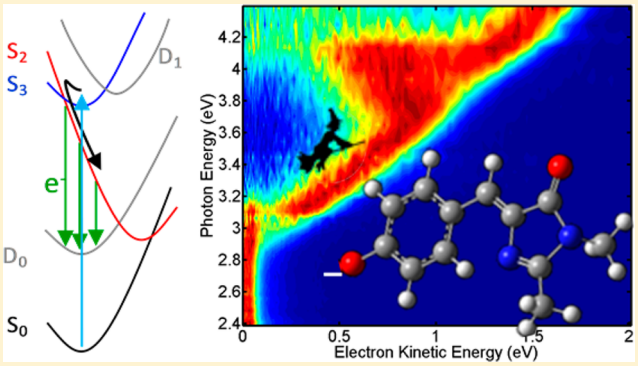


## INTRODUCTION

Over the past half-century, molecular biology has been revolutionized by the discovery of naturally occurring fluorescent proteins and their development into a fluorescent probe for *in vivo* biological imaging. The ability to incorporate a fluorescent probe into the genetic encoding of a protein without affecting the biological functionality imparts an unprecedented level of locational specificity that is unachievable with traditional fluorescent probes.[1−5] Of the fluorescent proteins, the green fluorescent protein (GFP) was the first discovered and remains the most widely utilized. The origins of the optical properties of GFP, as well as many other fluorescent proteins, can be traced to a chromophore enclosed deep within the $\beta$-barrel of the body of the protein.[6,7] In GFP, the chromophore is essentially identical to the deprotonated anion of *para*-hydroxybenzilidene-2,3-dimethylimidazolinone ($HBDI^-$, shown as inset in Figure 1f) and has been widely employed as a model to investigate the intrinsic photophysics of the chromophore within the protein.[8−18] In the gas phase, the $S_1$ state has been well-characterized: the $S_1 \leftarrow S_0$ absorption (action) spectrum is similar to that of the protein and its origin is vertically bound relative to the ground state of the neutral ($D_0$).[8,16] The $S_1$ state decays primarily by internal conversion on a time scale of 1.4 ps;[14] vibrational autodetachment is also an open channel, although this occurs on a 30 ps time scale.[18] Recently, the next optically accessible excited state of the anion, which is formally the $S_3$ excited state, has been considered. The action spectrum of $HBDI^-$ suggests that the $S_3 \leftarrow S_0$ transition is almost as bright as the $S_1 \leftarrow S_0$ transition and has an onset of ~3.8 eV in the gas phase.[9] Bochenkova et al. suggest that these states may be important in the photo-oxidation of GFP as the $S_3$ band of the protein in an aqueous solution is quasi-resonant with the hydrated electron.[9] In isolation, the $S_3$ state is a resonance and three photoelectron (PE) spectra recorded with photon energies around the onset of the $S_3$ state indicate that the PE distribution broadens with increasing photon energy.[15] This spectral broadening was assigned to vibrational motion on the $S_3$ excited state surface, followed by autodetachment to a range of coordinates of the neutral $D_0$ state.[15] In order to gain a more comprehensive understanding of the dynamics occurring in the continuum of $HBDI^-$ around the $S_3$ state, we have performed a frequency-, angle-, and time-resolved PE spectroscopy study that probes these dynamics in detail and shows that the primary decay mechanism is internal conversion.

## EXPERIMENTAL METHODS

The experiment has been described in detail elsewhere.[19−21] Briefly, $HBDI^-$ anions were produced by electrospray ionization of a ~1 mM solution of HBDI in methanol that was regulated to pH 10 by addition of $NH_3$. The free $HBDI^-$ ions are trapped in a radio frequency ring-electrode ion trap operating at ambient temperature (~300 K). The ion packet was injected into a time-of-flight mass spectrometer, and mass-selected $HBDI^-$ was irradiated at the center of a penetrating-field velocity-map-imaging assembly. In the frequency-resolved PE imaging experiments, laser pulses of ~6 ns duration with photon energies ranging between 2.38 eV (520 nm) and 4.39 eV (282 nm) were generated using an optical parametric oscillator pumped by a Nd:YAG laser. In the time-resolved experiments, femtosecond pulses at 4.13 eV (300 nm) were

Received: February 11, 2015
Revised: February 16, 2015
Published: February 16, 2015





DOI: 10.1021/acs.jpcb.5b01432
J. Phys. Chem. B 2015, 119, 3982−3987

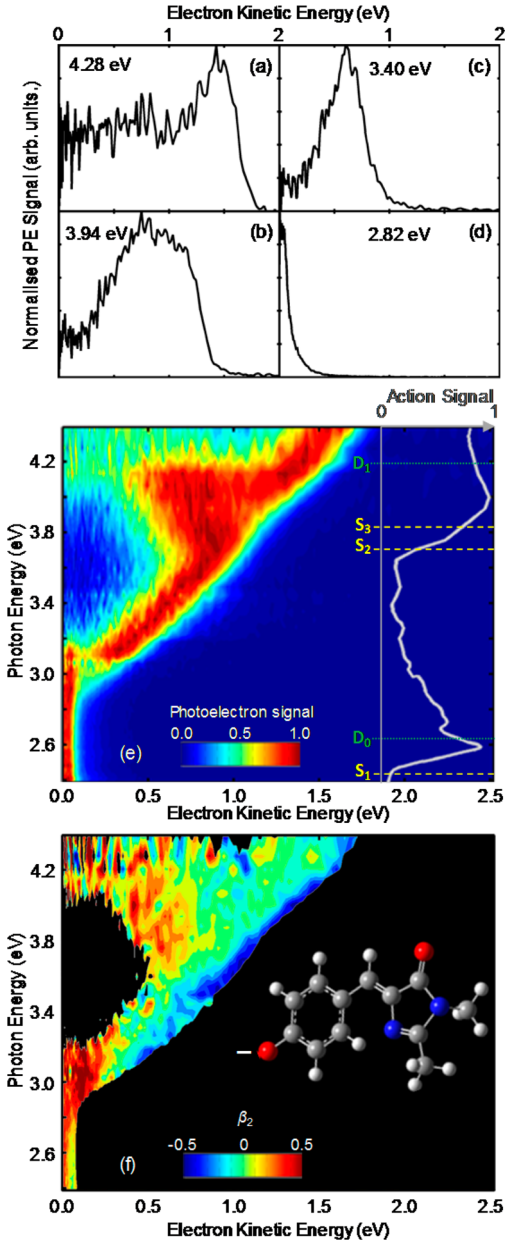


**Figure 1.** Frequency- and angle-resolved photoelectron (PE) spectra of $HBDI^-$. Representative PE spectra are shown in parts a–d. The complete set of peak-normalized PE spectra is shown in part e, together with the action spectrum and calculated energies, taken from ref 9. The PE anisotropy parameters are shown in part f with the structure of $HBDI^-$ inset.

used as the pump and 1.55 eV (800 nm) were used as the probe pulse. All time-resolved laser pulses were derived from a commercial femtosecond system. The 4.13 eV pump was generated by frequency doubling the 1.55 eV fundamental in a $\beta$-barium borate (BBO) crystal and combining this in a second BBO crystal with 1.03 eV (1200 nm) pulses produced by an optical parameter amplifier. PE spectra were extracted from the raw velocity-map images using a polar onion peeling algorithm,[22] and were calibrated using the known spectrum of $I^-$. The experimental resolution is around 5% and the cross-correlation between pump and probe pulses was 75 fs, offering a temporal resolution of ~40 fs.

## RESULTS AND ANALYSIS

Representative examples of PE spectra are shown in Figure 1a–d, while Figure 1e summarizes all frequency-resolved PE spectra of $HBDI^-$ for photon energies between 2.39 and 4.39 eV (48 individual PE spectra in the Supporting Information). The PE spectra have been normalized to have a maximum intensity of unity, which accentuates the spectral changes as a function of photon energy. The absolute PE yield, however, is strongly modulated across this range because of the variations in photoinduced detachment cross sections. To highlight this variation, the action (absorption) spectra leading to "prompt" electron loss as reported in the recent study of Bochenkova et al. are also shown, together with their calculated energetics of relevant electronic states.[9]

Despite $HBDI^-$ having an observed adiabatic detachment energy of 2.7 eV,[10,12,23] PE signal was observed between 2.39 eV < $h\nu$ < 2.70 eV, although signal levels rapidly became very weak at the lower photon energies. This below-threshold contribution is facilitated by the ~300 K temperature of the anions in our experiment, which corresponds to an internal energy of ~310 meV. The PE spectra in this range are all essentially identical (independent of photon energy) and consist of a peak centered at $eKE$ ~ 0.03 eV and a feature decaying exponentially from $eKE$ = 0 eV. These features remain identifiable up to $h\nu$ = 3.1 eV. However, from $h\nu$ = 2.8 eV, a new PE peak is observed at higher $eKE$ that increases linearly with photon energy, as might be expected for a direct (vertical) detachment process. For $h\nu$ > 3.7 eV, however, the $eKE$ distribution broadens with increasing photon energy, reaching a spectral width of $eKE$ ~ 1 eV at $h\nu$ ~ 4.1 eV. The high energy edge of this PE feature remains linear with photon energy, but the average $eKE$ of the spectrum shifts to increasingly lower energy to yield a bimodal distribution. In fact, the low energy side of this bimodal distribution remains approximately constant in $eKE$ with increasing $h\nu$, as can be seen more clearly from the individual PE spectra shown in the Supporting Information. The maximum of the low energy peak is around $eKE$ ~ 0.6 eV. For $h\nu$ > 4.1 eV, the progressively broadening feature abruptly collapses to a PE spectrum that has a feature consistent with direct detachment as well as a very broad and featureless distribution of electrons (0 eV < $eKE$ < 1.3 eV). The relative intensity of this broad distribution is lower than the low energy peak observed for 3.7 eV < $h\nu$ < 4.1 eV; however, their integrated PE yields are approximately the same. The broadened feature contributes about 60% of the total PE yield, with the other 40% arising from the constant binding energy PE feature at high $eKE$ (see the Supporting Information).

In addition to the frequency-resolved PE spectra, the photoejection anisotropy parameter, $\beta_2$, which quantifies the PE angular distribution,[24] is plotted in Figure 1f. These show that there is a small but consistent difference in $\beta_2(eKE)$ for the peak correlated with a direct detachment process and the feature at lower $eKE$ in the 3.7 eV < $h\nu$ < 4.1 eV range. In the 3.2 eV < $h\nu$ < 3.6 eV range, the sole PE peak with constant binding energy has $\beta_2$ ~ 0, and remains this value for $h\nu$ > 3.6 eV. Around $h\nu$ ~ 3 eV and between 0.1 eV < eV $eKE$ < 0.2 eV, the PE anisotropy is $\beta_2$ ~ 0.4.

The spectral broadening of the PE spectra over the 3.7 eV < $h\nu$ < 4.1 eV range suggests that excited state dynamics are occurring in competition with autodetachment. This broadening was previously assigned to vibrational motion on the $S_3$


DOI: 10.1021/acs.jpcb.5b01432
J. Phys. Chem. B 2015, 119, 3982–3987

state.[15] However, the spectral broadening could also arise from internal conversion of the $S_3$ state to the lower-lying $S_2$ state followed by autodetachment. The $S_2$ state has a calculated energy that lies within 0.1 eV of the $S_3$ state,[9] suggesting that pathways of coupling these two states may be present.

In order to glean further insight into the decay mechanisms, the dynamics of the $S_3$ state were probed using time-resolved PE spectroscopy. In these experiments, the $S_3$ excited state was populated using femtosecond photoexcitation at 4.1 eV (300 nm), which was subsequently probed at 1.55 eV (800 nm). The excitation energy was chosen to energetically coincide with the spectral broadening observed in the 3.7 eV < $h\nu$ < 4.1 eV region of the frequency-resolved PE spectra as well as the local maximum in PE yield from the action spectra.

Figure 2a shows two representative pump−probe PE spectra recorded with the probe arriving before pump pulses ($\Delta t$ = −525 fs) and near the temporal overlap of the two pulses ($\Delta t$ = 25 fs). Both spectra show two peaks centered at ∼0.25 and ∼1.28 eV. The appearance of the PE spectrum between 0.5 eV < *eKE* < 1.5 eV is consistent with the 4.1 eV (300 nm) PE spectrum obtained in the frequency-resolved experiments. The peak at *eKE* ∼ 0.25 eV arises from a nonresonant two-photon detachment process from the 1.55 eV probe; the PE spectrum at *eKE* < 0.5 eV is consistent with the PE spectrum recorded at 3.1 eV (400 nm). At $\Delta t \sim 0$, an additional PE feature between 1.5 eV < *eKE* < 3.0 eV is observed. This can be assigned to photodetachment from the excited state population; the PE spectrum of the time-dependent feature extends approximately an additional 1.55 eV beyond that of the pump-only PE spectrum. The breadth of the time-dependent PE feature suggests that it contains contributions from both excited state populations, leading to both prompt autodetachment (high *eKE* electrons) and delayed autodetachment (lower *eKE*).

To gain quantitative insight, the time-dependent PE feature can be divided into two spectral windows, as shown in Figure 2a. The 2.5 eV < *eKE* < 3.0 eV window probes the population of the initially excited state, and the 1.5 eV < *eKE* < 2.5 eV window probes the population of the intermediate state to which the initial state has decayed. The time-varying integrated PE signals for each of these spectral windows are given in Figure 2b and were fitted to an exponential decay function, $f(t) = A\exp(-(t - t_0)/\tau)$, convoluted with the instrument response function (fwhm = 75 fs). The amplitude ($A$), lifetime ($\tau$), and time-zero ($t_0$) were allowed to vary. The $t_0$ for both spectral windows were less than 5 fs apart and can be assumed to be essentially identical. The lifetime of the initially excited state was found to be 25 fs, which is less than our temporal resolution and so we may only quote this as <40 fs. The lifetime of the intermediate state was found to be 55 fs, which is still extremely fast, although visibly slower than that of the initially excited state.

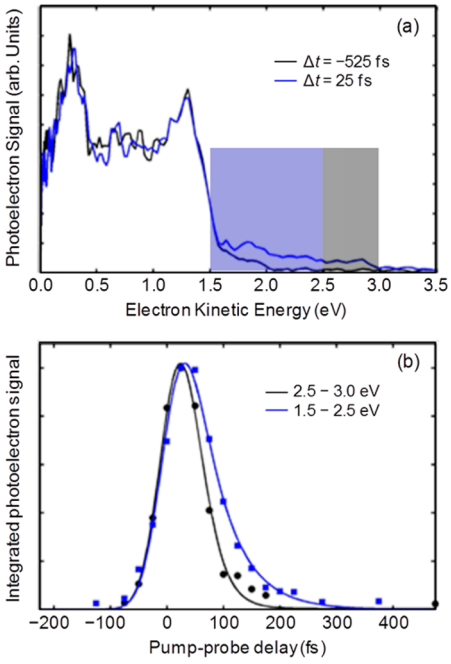


**Figure 2.** (a) Time-resolved photoelectron (PE) spectra of $HBDI^-$ excited at 4.1 eV. (b) Decay dynamics of PE signal taken over the spectral windows shown in part a.

## DISCUSSION

The PE peak at *eKE* = 0.03 eV in the range 2.6 eV < $h\nu$ < 3.1 eV has previously been assigned to vibrational autodetachment (VAD) from the $S_1$ excited state.[8] The exponential tail decaying from *eKE* = 0 eV has been correlated with statistical (thermionic) electron emission.[12] These features remain identifiable up to $h\nu \sim 3.1$ eV. However, from $h\nu$ > 2.8 eV, a new PE peak is observed at higher *eKE*. This new feature corresponds to direct photodetachment into the continuum. Between 2.8 eV < $h\nu$ < 3.1 eV, the two processes are in competition and VAD is dominant because the $S_1$ state is predominantly excited. In the higher energy window, 3.2 eV < $h\nu$ < 3.7 eV, the cross section for excitation to the $S_1$ sharply decreases and the PE signal is probably dominated by direct detachment. The photoejection anisotropy is significantly more positive around $h\nu \sim 3.1$ eV, as shown in Figure 1f. This might be a consequence of the interference between autodetachment and direct detachment into the continuum leading to a different $\beta_2$ value than that for exclusively direct detachment, which is dominant for 3.2 eV < $h\nu$ < 3.7 eV.

The frequency-resolved PE spectra combined with the prompt action spectra from the Andersen group[9] show that for $h\nu$ > 3.7 eV higher-lying excited states are accessed. Using high-level calculations, Bochenkova et al. showed that the $S_2$ and $S_3$ are very close in energy at 3.7 and 3.8 eV, respectively, in the vertical Franck−Condon (FC) region (see Figure 1e). The increase in the action spectrum shows that the PE peak that is increasing linearly with photon energy for $h\nu$ > 3.7 eV is predominantly arising from an indirect detachment process. In Figure 3, we show the molecular orbital (MO) configurations of the relevant electronic states of $HBDI^-$ and its neutral, as calculated by Bochenkova et al.[9] To a first approximation, the MOs can be roughly classified into different types of localized MOs that are useful as a guide to further discussions. MO(7) is primarily of $\pi$ bonding character on the allyl moiety that couples the phenol to the imidazole rings. MO(8), which is the highest occupied MO (HOMO), is essentially nonbonding on the allyl bridge, while MO(9) has $\pi^*$ character. The $S_2 \leftarrow S_0$ transition is one in which $\pi$ bonding orbitals are replaced for antibonding orbitals over the allyl. Hence, the population of the $S_2$ state in the FC region is likely to involve rapid wavepacket motion, leading to a stretching of the allyl bridge. The $S_1 \leftarrow S_0$ transition is similar in that it has $\pi^*$ character on the allyl bridge, and the initial wavepacket dynamics of the allyl stretching mode on the $S_1$ state was predicted to be on the order of 10 fs.[25,26] For the $S_2$ state, the antibonding character is


DOI: 10.1021/acs.jpcb.5b01432
J. Phys. Chem. B 2015, 119, 3982−3987

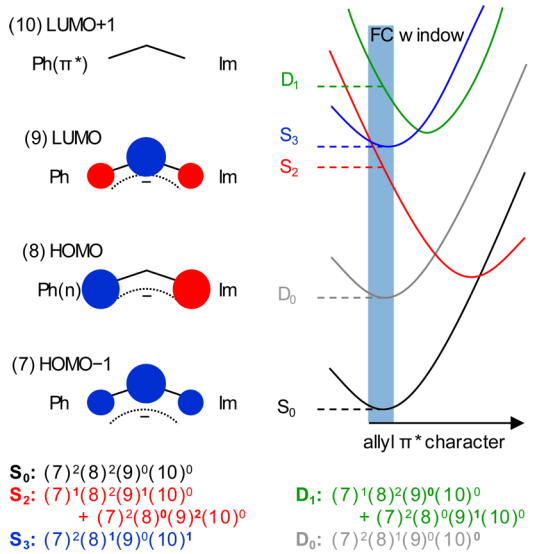


**Figure 3.** Left: Molecular orbitals of $HBDI^-$ with contributions to the central allyl bridge that connects the phenol (Ph) with the imidazole (Im) shown schematically. Right: Schematic of potential energy curves of the various anionic and neutral excited states considered as a function of allyl antibonding character. Below: Electronic configurations of the various electronic states, where the bold numbers indicate where electrons have been moved.

increased and one might expect the $S_2$ state to be more repulsive along the stretching coordinate of the allyl bridge (at the FC geometry) with initial nuclear wavepacket motion that is similar to or faster than that on the $S_1$ state. In contrast, the $S_3 \leftarrow S_0$ transition is one in which MO(8) is excited to MO(10), which is localized on the phenol ring. The main structural differences are thus expected to be on the phenol, and one might anticipate only modest structural changes along the allyl coordinate. Finally, we consider the neutral states, $D_0$ and $D_1$. The ground $D_0$ state corresponds to loss of an electron from MO(8). As MO(8) is essentially nonbonding on the allyl bridge, the $D_0$ state will have a similar minimum energy geometry to the $S_0$ state along the allyl stretching coordinate. Indeed, the PE feature for direct detachment is relatively sharp given the molecular size of HBDI.[12,23] The $S_3$ excited state is correlated with $D_0$ in a one-electron Koopmans picture; $S_3$ is a shape resonance, which typically exhibits a very short autodetachment lifetime (tens of femtoseconds). In contrast, the $S_2$ state does not correlate with the $D_0$ state (i.e., $S_2$ is a Feshbach resonance), but it is correlated with the $D_1$ excited state of the neutral. The above picture has been schematically summarized as potential energy curves along the allyl stretch ($\pi^*$ character) in Figure 3, and we will use this as a guide to understanding the dynamics that are evident in the frequency-resolved PE spectra.

The spectral broadening in the 3.7 eV < $h\nu$ < 4.1 eV range suggests that excited state dynamics are occurring before electron emission. The $S_3 \leftarrow S_0$ excitation is significantly brighter than the $S_2 \leftarrow S_0$ excitation; hence, we may assume that the $S_3$ state is initially populated in this range, and direct detachment is a very minor channel that can essentially be ignored. The observed broadening in the PE spectra could arise from vibrational dynamics on the $S_3$ state that precedes autodetachment, as suggested by Mooney et al.[15] Alternatively, because the $S_2$ state is in very close proximity to the $S_3$ state in the FC region, it is conceivable that there exists a strong coupling or conical intersection between these two states that can transfer population from $S_3$ to $S_2$ on a time scale faster than autodetachment. Such dynamics have indeed been observed in some quinone anions.[21,27,28]

The latter of the two scenarios above is more consistent with the experimental results. The PE angular distribution across the bimodal peak is not constant in the 3.7 eV ≥ $h\nu$ ≥ 4.1 eV range. The anisotropy over the high energy component is slightly negative ($\beta_2 \sim -0.3$), while that across the lower *eKE* portion is positive ($\beta_2 \sim +0.2$). Because the PE angular distribution depends sensitively on the MO from which the electron is detached, the difference in the anisotropy across the bimodal distribution reflects a change in the electronic character.[21] Additionally, the $S_3$ state minimum energy geometry is not expected to be very different from that of the $D_0$ state, so it would be difficult to reconcile the large spectral red-shift of (~0.8 eV) assuming vibrational motion occurring on a time scale of <40 fs. In contrast, the $S_2$ state is expected to have its minimum energy geometry far from the FC region because of the strong $\pi^*$ character on the allyl bridge. As a result, one might envisage that the $S_2$ and $D_0$ potential energy surfaces will be far from parallel along the allyl stretching coordinate, as shown schematically in Figure 3. Furthermore, the dynamics of along the allyl stretch are known to be very fast (10 fs).[25,26] Of course, these dynamics occurring on the $S_2$ state would be in competition with autodetachment. However, as the $S_2$ state is not correlated with the $D_0$ state, the $S_2 \rightarrow D_0$ autodetachment will be slower, allowing for the vibrational wavepacket to sample a larger area of the $S_2$ potential energy surface. This would in turn lead to a large spectral width in the PE emission as observed.

On the basis of the time-resolved PE spectra, the dynamics of the $S_3 \rightarrow S_2$ internal conversion is extremely fast (sub-40 fs). However, the internal conversion is also in competition with autodetachment from the $S_3$ state. This competition is evidenced in the frequency resolved spectra by the PE feature that increases linearly with *eKE* as the photon energy is increased. This PE feature is predominantly due to the $S_3 \rightarrow D_0$ autodetachment channel because direct detachment into the continuum is a minor channel in this energy range[9] (see the action spectrum in Figure 1e). From the frequency-resolved spectra, the PE yield due to $S_3 \rightarrow D_0$ autodetachment is ~40% of the total PE yield, with the remaining 60% arising from $S_2$ autodetachment (see the Supporting Information). On the basis of competing kinetics, internal conversion occurs on a <65 fs time scale, while $S_3 \rightarrow D_0$ autodetachment is slower. However, we note that the true lifetime will be significantly faster given that the $S_3 \rightarrow D_0$ autodetachment is a very favorable process, but it is limited by our time resolution. The spectral broadening observed over the 3.7 eV < $h\nu$ < 4.1 eV range can thus be assigned to vibrational dynamics on the $S_2$ state that leads to a broad PE spectrum in this range. The overall decay of this $S_2$ state feature occurs on a time scale of 55 fs, and can be correlated to the $S_2 \rightarrow D_0$ autodetachment.

Perhaps the most striking feature of the frequency-resolved PE spectra is that, at $h\nu$ > 4.1 eV, the PE spectra abruptly change from the bimodal distribution (between 3.7 eV < $h\nu$ < 4.1 eV) to a very broad distribution (see Figure 1a and b). This change is suggestive of a new decay pathway becoming available at this energy, and this happens to coincide with the calculated location of the $D_1$ excited state of the neutral in the FC region.[9] The $D_1$ state is not correlated with the $S_3$ state, but it is correlated with the $S_2$ state in a one-electron Koopmans'


DOI: 10.1021/acs.jpcb.5b01432
J. Phys. Chem. B 2015, 119, 3982−3987

interpretation (see Figure 3). Hence, we propose that, as the photon energy increases and becomes higher than the $D_1$ energy, autodetachment from the $S_2$ state becomes much faster by virtue of the favorable $S_2 \rightarrow D_1$ autodetachment channel. Indeed, it can be seen in the frequency-resolved PE spectra, and more clearly in the PE spectra at $h\nu$ = 4.28 eV and $h\nu$ = 3.94 eV (Figure 1a and b), that the peak around *eKE* ∼ 0.6 eV, that can be assigned to $S_2 \rightarrow D_0$ autodetachment, relative to the peak arising from $S_3 \rightarrow D_0$ autodetachment is decreasing. Concomitantly, a new feature emerges at lower *eKE*.

For completeness, we consider the alternative scenario in which the $S_2$ state plays no role in the dynamics. In this case, all dynamics observed between 3.7 eV < $h\nu$ < 4.1 eV would be occurring on the $S_3$ state. The change in PE spectra at $h\nu$ = 4.1 eV could then be assigned to either a conical intersection with the $S_2$ state that becomes available at this energy or the opening of the $S_3 \rightarrow D_1$ autodetachment channel. The problem with the latter is that the $S_3$ state is not correlated with the $D_1$ state. Additionally, in either case, one would expect that the PE yield in the $S_3 \rightarrow D_0$ autodetachment channel (peak at highest *eKE*) would transfer to a lower *eKE* and this is not experimentally observed. Instead, the contribution of the $S_3 \rightarrow D_0$ autodetachment channel to the total PE yield does not change between $h\nu$ = 3.9 and 4.3 eV (see the Supporting Information) and PE intensity in the feature at *eKE* ∼ 0.6 eV migrates to the feature at lower *eKE*. Therefore, only the population that has first undergone internal conversion from the $S_3$ excited state is involved in detachment through the new channel. Finally, one could interpret the bimodal feature as being composed of $S_3 \rightarrow D_0$ (peak at *eKE* ∼ 0.6 eV) and direct $S_0 \rightarrow D_0$ detachment (peak increasing linearly in *eKE* with $h\nu$), as done by Mooney et al. However, on the basis of the integrated electron yields in these channels, this would suggest that the cross section for $S_3 \leftarrow S_0$ excitation relative to direct $S_0 \rightarrow D_0$ detachment is ∼3:2. This is completely inconsistent with the absorption spectrum shown in Figure 1e, which clearly shows that the absorption cross section is ∼10 times greater than direct detachment. Thus, the experimental data, when viewed holistically, strongly points to a process in which the initial $S_3$ population rapidly converts to the $S_2$ state.

## SUMMARY

In summary, using frequency-, angle-, and time-resolved photoelectron spectroscopy, we have assigned the dynamics following UV excitation of the chromophore anion of the green fluorescent protein and this is summarized in Figure 4. Excitation with $h\nu$ > 3.7 eV leads to the population of the bright $S_3$ excited state that decays through a combination of autodetachment to the $D_0$ ground neutral state and internal conversion to the nearby $S_2$ excited state, with the latter having a higher yield. The subsequent dynamics on the $S_2$ state involve rapid vibrational motion that is in competition with autodetachment from the $S_2$ state to the $D_0$ neutral ground state. When $h\nu \geq$ 4.1 eV, the $S_2 \rightarrow D_1$ autodetachment channel opens up and this is favored over the $S_2 \rightarrow D_0$ channel based on a Koopmans' interpretation. In GFP, the excited states cannot autodetach, as the vacuum is replaced by a protein that is surrounded by water.[29] Bochenkova et al. showed that the UV excited states are quasi-resonant with the hydrated electron in aqueous GFP such that autodetachment could be replaced by charge transfer, which could lead to photo-oxidation of the chromophore.[9] In the limit that the isolated $HBDI^-$ has a similar electronic structure in GFP, our results suggest that this pathway will not be very efficient because population of the optically bright $S_3$ state rapidly converts to the $S_2$ state. Although the dynamics on $S_2$ lead to a broad spectrum that will enhance overlap with the hydrated electron state(s), one would also expect a very weak coupling between the donor and acceptor states. This is because the $S_2$ state is correlated with the $D_1$ excited neutral state and charge transfer would require a two-electron transition. Nevertheless, the lifetime of the $S_2$ state in the protein may be sufficiently long to enable charge transfer. We stress that these arguments are based on the assumption that the $S_n$ excited states of gas-phase $HBDI^-$ are similar in the protein, which requires further investigation; however, UV excitation in the protein is experimentally complicated by the fact that several protein residues also absorb in this range. Hence, gas-phase studies provide an important portal to explore the UV excited photophysics of GFP.

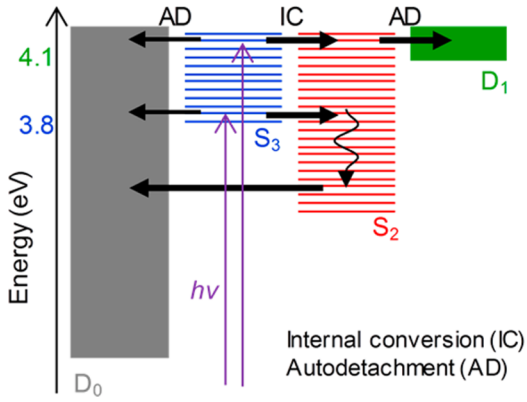


**Figure 4.** Summary of the dynamics occurring in $HBDI^-$ following excitation below and above the onset of the $D_1$ excited state. The black horizontal arrows indicate the competing processes, and their thickness reflects their respective rates.

## ASSOCIATED CONTENT

### Supporting Information

Discussion of photoelectron (PE) yields in the different autodetachment channels; individual PE spectra that make up Figure 1e. This material is available free of charge via the Internet at http://pubs.acs.org.

## AUTHOR INFORMATION

### Corresponding Author

*E-mail: j.r.r.verlet@durham.ac.uk.

### Notes

The authors declare no competing financial interest.

## ACKNOWLEDGMENTS

Funding was provided by the ERC (Starting Grant 306536).

## REFERENCES

(1) Cubitt, A. B.; Heim, R.; Adams, S. R.; Boyd, A. E.; Gross, L. A.; Tsien, R. Y. Understanding, Improving and Using Green Fluorescent Proteins. *Trends Biochem. Sci.* **1995**, *20*, 448−455.

(2) Lippincott-Schwartz, J.; Patterson, G. H. Development and Use of Fluorescent Protein Markers in Living Cells. *Science* **2003**, *300*, 87−91.

(3) Patterson, G. H.; Knobel, S. M.; Sharif, W. D.; Kain, S. R.; Piston, D. W. Use of the Green Fluorescent Protein and Its Mutants in Quantitative Fluorescence Microscopy. *Biophys. J.* **1997**, *73*, 2782−2790.



DOI: 10.1021/acs.jpcb.5b01432
*J. Phys. Chem. B* 2015, 119, 3982−3987

(4) Tsien, R. Y. The Green Fluorescent Protein. *Annu. Rev. Biochem.* **1998**, *67*, 509−544.
(5) Zimmer, M. Green Fluorescent Protein (GFP): Applications, Structure, and Related Photophysical Behavior. *Chem. Rev.* **2002**, *102*, 759−781.
(6) Yang, F.; Moss, L. G.; Phillips, G. N. The Molecular Structure of Green Fluorescent Protein. *Nat. Biotechnol.* **1996**, *14*, 1246−1251.
(7) Cody, C. W.; Prasher, D. C.; Westler, W. M.; Prendergast, F. G.; Ward, W. W. Chemical-Structure of the Hexapeptide Chromophore of the Aequorea Green-Fluorescent Protein. *Biochemistry* **1993**, *32*, 1212−1218.
(8) Bochenkova, A.; Andersen, L. Ultrafast Dual Photoresponse of Isolated Biological Chromophores: Link to the Photoinduced Mode-Specific Non-Adiabatic Dynamics in Proteins. *Faraday Discuss.* **2013**, *163*, 297−319.
(9) Bochenkova, A. V.; Klaerke, B.; Rahbek, D. B.; Rajput, J.; Toker, Y.; Andersen, L. H. UV Excited-State Photoresponse of Biochromophore Negative Ions. *Angew. Chem., Int. Ed.* **2014**, *53*, 9797−9801.
(10) Bravaya, K. B.; Krylov, A. I. On the Photodetachment from the Green Fluorescent Protein Chromophore. *J. Phys. Chem. A* **2013**, *117*, 11815−11822.
(11) Forbes, M. W.; Jockusch, R. A. Deactivation Pathways of an Isolated Green Fluorescent Protein Model Chromophore Studied by Electronic Action Spectroscopy. *J. Am. Chem. Soc.* **2009**, *131*, 17038−17039.
(12) Horke, D. A.; Verlet, J. R. R. Photoelectron Spectroscopy of the Model Gfp Chromophore Anion. *Phys. Chem. Chem. Phys.* **2012**, *14*, 8511−8515.
(13) Litvinenko, K. L.; Webber, N. M.; Meech, S. R. Internal Conversion in the Chromophore of the Green Fluorescent Protein: Temperature Dependence and Isoviscosity Analysis. *J. Phys. Chem. A* **2003**, *107*, 2616−2623.
(14) Mooney, C. R. S.; Horke, D. A.; Chatterley, A. S.; Simperler, A.; Fielding, H. H.; Verlet, J. R. R. Taking the Green Fluorescence out of the Protein: Dynamics of the Isolated GFP Chromophore Anion. *Chem. Sci.* **2013**, *4*, 921−927.
(15) Mooney, C. R. S.; Parkes, M. A.; Zhang, L.; Hailes, H. C.; Simperler, A.; Bearpark, M. J.; Fielding, H. H. Competition between Photodetachment and Autodetachment of the $2^1\pi\pi^*$ State of the Green Fluorescent Protein Chromophore Anion. *J. Chem. Phys.* **2014**, *140*, 205103.
(16) Nielsen, S. B.; Lapierre, A.; Andersen, J. U.; Pedersen, U. V.; Tomita, S.; Andersen, L. H. Absorption Spectrum of the Green Fluorescent Protein Chromophore Anion *in Vacuo*. *Phys. Rev. Lett.* **2001**, *87*, 228102.
(17) Toker, Y.; Rahbek, D. B.; Klaerke, B.; Bochenkova, A. V.; Andersen, L. H. Direct and Indirect Electron Emission from the Green Fluorescent Protein Chromophore. *Phys. Rev. Lett.* **2012**, *109*, 128101.
(18) West, C. W.; Hudson, A. S.; Cobb, S. L.; Verlet, J. R. R. Communication: Autodetachment Versus Internal Conversion from the $S_1$ State of the Isolated GFP Chromophore Anion. *J. Chem. Phys.* **2013**, *139*, 071104.
(19) Lecointre, J.; Roberts, G. M.; Horke, D. A.; Verlet, J. R. R. Ultrafast Relaxation Dynamics Observed through Time-Resolved Photoelectron Angular Distributions. *J. Phys. Chem. A* **2010**, *114*, 11216−11224.
(20) Horke, D. A.; Roberts, G. M.; Lecointre, J.; Verlet, J. R. R. Velocity-Map Imaging at Low Extraction Fields. *Rev. Sci. Instrum.* **2012**, *83*, 063101.
(21) West, C. W.; Bull, J. N.; Antonkov, E.; Verlet, J. R. R. Anion Resonances of *Para*-Benzoquinone Probed by Frequency-Resolved Photoelectron Imaging. *J. Phys. Chem. A* **2014**, *118*, 11346−11354.
(22) Roberts, G. M.; Nixon, J. L.; Lecointre, J.; Wrede, E.; Verlet, J. R. R. Toward Real-Time Charged-Particle Image Reconstruction Using Polar Onion-Peeling. *Rev. Sci. Instrum.* **2009**, *80*, 053104.
(23) Deng, S. H. M.; Kong, X.-Y.; Zhang, G.; Yang, Y.; Zheng, W.-J.; Sun, Z.-R.; Zhang, D.-Q.; Wang, X.-B. Vibrationally Resolved Photoelectron Spectroscopy of the Model GFP Chromophore Anion Revealing the Photoexcited $S_1$ State Being Both Vertically and Adiabatically Bound against the Photodetached $D_0$ Continuum. *J. Phys. Chem. Lett.* **2014**, *5*, 2155−2159.
(24) Reid, K. L. Photoelectron Angular Distributions. *Annu. Rev. Phys. Chem.* **2003**, *54*, 397−424.
(25) Martin, M. E.; Negri, F.; Olivucci, M. Origin, Nature, and Fate of the Fluorescent State of the Green Fluorescent Protein Chromophore at the CASPT2//CASSCF Resolution. *J. Am. Chem. Soc.* **2004**, *126*, 5452−5464.
(26) Zhao, L.; Zhou, P.-W.; Li, B.; Gao, A.-H.; Han, K.-L. Non-Adiabatic Dynamics of Isolated Green Fluorescent Protein Chromophore Anion. *J. Chem. Phys.* **2014**, *141*, 235101.
(27) Horke, D. A.; Li, Q.; Blancafort, L.; Verlet, J. R. R. Ultrafast above-Threshold Dynamics of the Radical Anion of a Prototypical Quinone Electron-Acceptor. *Nat. Chem.* **2013**, *5*, 711−717.
(28) Bull, J. N.; West, C. W.; Verlet, J. R. R. On the Formation of Anions: Frequency-, Angle-, and Time-Resolved Photoelectron Imaging of the Menadione Radical Anion. *Chem. Sci.* **2015**, *6*, 1578−1589.
(29) Bravaya, K. B.; Khrenova, M. G.; Grigorenko, B. L.; Nemukhin, A. V.; Krylov, A. I. Effect of Protein Environment on Electronically Excited and Ionized States of the Green Fluorescent Protein Chromophore. *J. Phys. Chem. B* **2011**, *115*, 8296−8303.


DOI: 10.1021/acs.jpcb.5b01432
*J. Phys. Chem. B* 2015, 119, 3982−3987